Emergence and Control of Stacking Fault Formation during Nanoparticle Cation Exchange Reactions

Auston G. Butterfield,[1] Lucas T. Alameda,[1] Raymond E. Schaak[1,2,3]*

[1] Department of Chemistry, [2] Department of Chemical Engineering, and [3] Materials Research Institute, The Pennsylvania State University, University Park, PA 16802

ABSTRACT: Cation exchange reactions modify the composition of a nanocrystal while retaining other features, including crystal structure and morphology. In many cases, the anion sublattice is considered to be locked in place as cations rapidly shuttle in and out. Here, we show evidence that the anion sublattice can shift significantly during nanocrystal cation exchange reactions. When the Cu^+ cations of roxbyite $Cu_{1.8}S$ nanorods exchange with Zn^{2+} to form ZnS nanorods, a high density of stacking faults emerge. During cation exchange, the stacking sequence of the close-packed anion sublattice shifts at many locations to generate a nanorod product containing a mixture of wurtzite, zincblende, and a wurtzite/zincblende polytype that contains an ordered arrangement of stacking faults. Reagent concentration and reaction temperature, which control the cation exchange rate, serve as synthetic levers that can tune the stacking fault density from high to low, which is important because once introduced, the stacking faults could not be modified through thermal annealing. This level of synthetic control through nanocrystal cation exchange is important for controlling properties that depend on the presence and density of stacking faults.

Cation exchange reactions are increasingly used to synthesize colloidal nanoparticles having otherwise inaccessible features and complexity that is unmatched by other mainstream methods that are high-yield and scalable.[1-5] In these reactions, the highly mobile cations in a parent nanoparticle are replaced with guest cations from solution. The anion sublattice is often preserved during these reactions.[2,6] This crystal structure retention is a prerequisite to accessing metastable crystal structures and achieving complex heterostructuring.[2-5,7-8] For example, roxbyite copper sulfide ($Cu_{1.8}S$) has a distorted hexagonal close packed (hcp) anion sublattice, and replacing the Cu^+ cations in roxbyite nanospheres with Zn^{2+} produces wurtzite ZnS, which also has an hcp anion sublattice.[7,9] The assumption is that the anion sublattice is rigid on the timescale of cation diffusion. This rigidity allows the cations to be replaced while the anion sublattice remains unchanged, although hints that the anion sublattice may be more dynamic are beginning to emerge.[8,10-14]

Here, we show evidence that the close-packed planes can slip and significantly rearrange their stacking sequences during complete exchange of the Cu^+ cations in roxbyite $Cu_{1.8}S$ nanorods with Zn^{2+} to form ZnS. This behavior produces a high density of periodic stacking faults that bridge wurtzite, which has an hcp anion sublattice, and zincblende, which has a cubic close packed (ccp) anion sublattice. Wurtzite and zincblende differ in the vertical stacking of their close-packed planes – ABAB for wurtzite and ABCABC for zincblende. Stacking faults in these polymorphic systems made through direct growth are well known, as there is little energetic difference between deposition of ABC *vs* ABA layer sequences.[15-19] While a few stacking faults have been observed during some cation exchange reactions[9,10,20], the emergence of a high-density of stacking faults is unexpected, since the stacking sequence of the close-packed planes is already locked in place through the structure of the copper sulfide precursor. The post-synthetic introduction of stacking faults would require many local anion

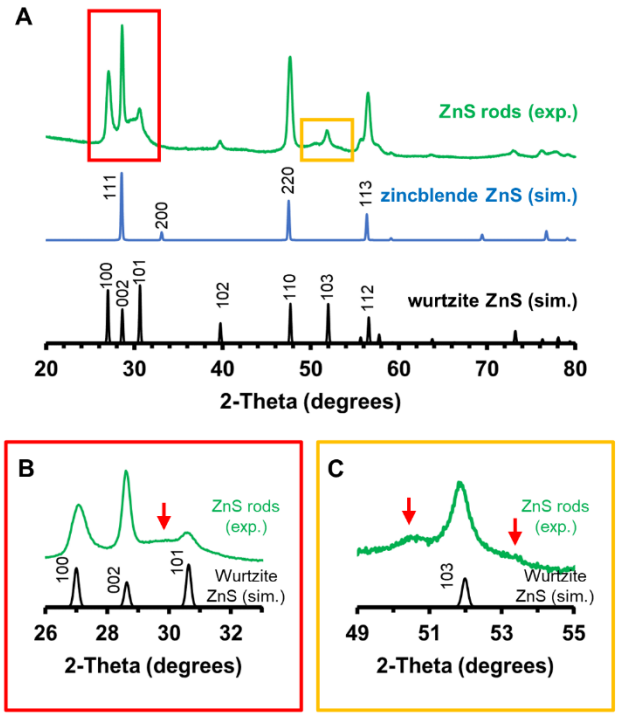

Figure 1. A) Experimental XRD pattern (top) for ZnS nanorods and simulated patterns for zincblende (middle) and wurtzite (bottom) ZnS. Expanded regions highlight key discrepancies between the experimental pattern and wurtzite ZnS, including the broad peaks at (B) 29 º2θ and (C) 50.5 and 53 º2θ (red arrows).

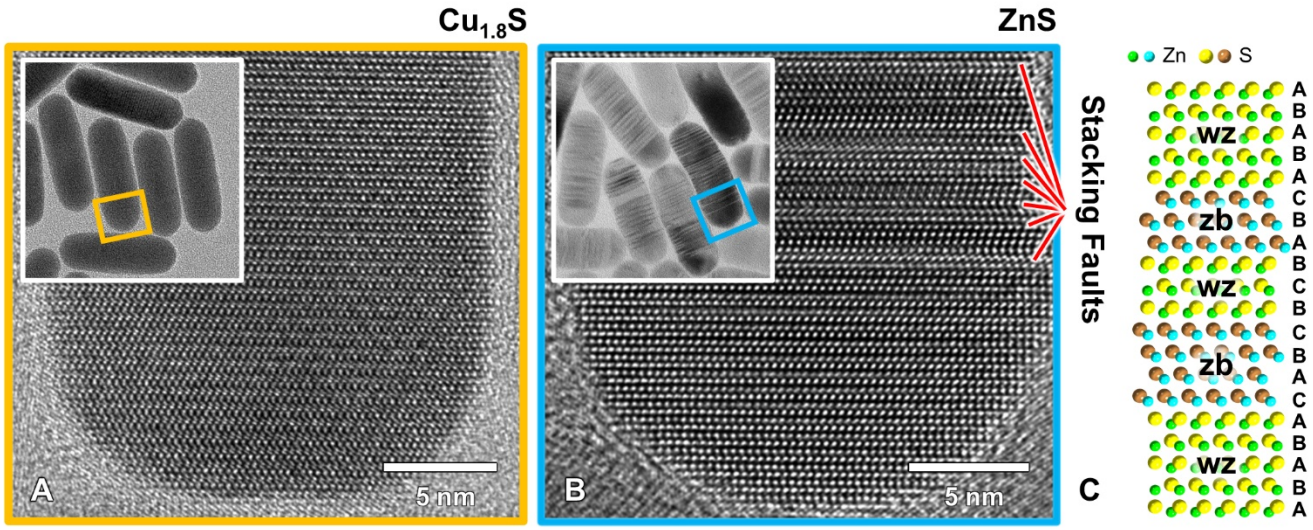

Figure 2. TEM and HRTEM images of (A) $Cu_{1.8}S$ precursor and (B) ZnS product nanorods. (C) Crystallographic model of stacking faults resulting from hcp wurtzite (wz) layers transitioning to ccp zincblende (zb).

sublattice rearrangements. Because stacking faults can influence properties, understanding how they form and can be controlled is important.[21-24]

To synthesize ZnS nanorods, an exchange solution of $ZnCl_2$ in benzyl ether, oleylamine, and octadecene was rapidly injected into a suspension of roxbyite $Cu_{1.8}S$ nanorods (Figure S1) in the same solvents at 120 ºC; experimental details are in the Supporting Information. Complete exchange of Cu^+ for Zn^{2+} (Figure S2-3) occurred almost immediately, based on the rapid color change from brown to white.[25] Figure 1 shows XRD data for the ZnS nanorods. While the peak positions match well with those for wurtzite ZnS, which is the expected Zn^{2+} exchange product of roxbyite due to hcp sublattice retention,[7] there are three notable discrepancies. First, the wurtzite peaks that overlap with zincblende peaks have significantly higher intensities than the wurtzite pattern alone would predict. Second, the relative intensities of the <101> family of planes are lower than expected. Third, the signal does not return to the expected background levels at several places, including between the wurtzite (002) and (101) peaks and on either side of the wurtzite (103) peak.

TEM images of the roxbyite nanorods (Figure 2A) show that they are single crystalline with uniform contrast throughout. The ZnS nanorods, however, exhibit high-contrast stripes along the nanorod lengths (Figure 2B). Such stripes are often the result of strain, which can occur at the interface between two phases. This is common for wurtzite and zincblende, and is typically diagnostic of stacking faults.[26-27] The HRTEM images in Figures 2B and S4 show both wurtzite and zincblende regions, based on the measured d-spacings and analysis of the stacking sequences of the close-packed planes, and confirm the presence of stacking faults, which are not present in the $Cu_{1.8}S$ precursor. A depiction of the local structure, showing the stacking faults created from various alternating regions of wurtzite and zincblende, is shown in Figure 2C.

Upon confirming the presence of stacking faults, we used DIFFaX[28] to construct a simulated XRD pattern based on a wurtzite ZnS structural model that contained various combinations of stacking faults (Table S1). A model consisting of hcp (wurtzite) ZnS with 25% randomly occurring ccp (zincblende) close-packed planes (Figure 3A) accounted for the peak broadening and the suppression of <101> peaks observed in the experimental XRD pattern, but not the broad peaks near 29, 50.5, and 53 º2θ. Further analysis revealed that the broad peak at 29 º2θ, as well as tailing of the wurtzite (100) peak at 27 º2θ, was captured by a ZnS polytype (Figure 3A). Polytypes have an ordered, periodic arrangement of stacking faults. Approximately 200 unique ZnS polytypes are known, and it is difficult to unambiguously assign our data to one of these, since they are closely related. However, certain polytypes occur more frequently than others, and most ZnS polytypes can be classified into one of three space groups and differ only subtly in their stacking sequences; their XRD patterns therefore appear similar.[29-30] The polytype associated with PDF card 04-009-3285 (Figure 3B) matches well and was incorporated into the structural model to improve the fit with the experimental XRD data.[31]

Figure 3A shows a simulated XRD pattern for a model that includes a three-phase mixture: 67% is the previously described DIFFaX structure containing wurtzite ZnS with 25% random zincblende stacking faults, 26% is the ZnS polytype (PDF card 04-009-3285), and 7% is pure wurtzite ZnS, as TEM images consistently show regions of pure wurtzite ZnS at the nanorod tips. We speculate that the tips remain free of stacking faults because of their higher surface area, as wurtzite is the favored polymorph at smaller sizes based on surface energetics.[16,32] It is also possible that the tips, which are thinner than the body of the nanorod, allow any stacking faults to slip so that they re-form the preferred wurtzite phase.[15,29] As can be seen in the HRTEM images in Figure 3C and S5, random stacking faults, regions of ordered stacking faults, and pure wurtzite tips are observed, which matches the DIFFaX model and XRD data. Additionally, the model includes 0.5% strain broadening to account for broadening caused by the high density of planar defects at the nanoscale.[27]

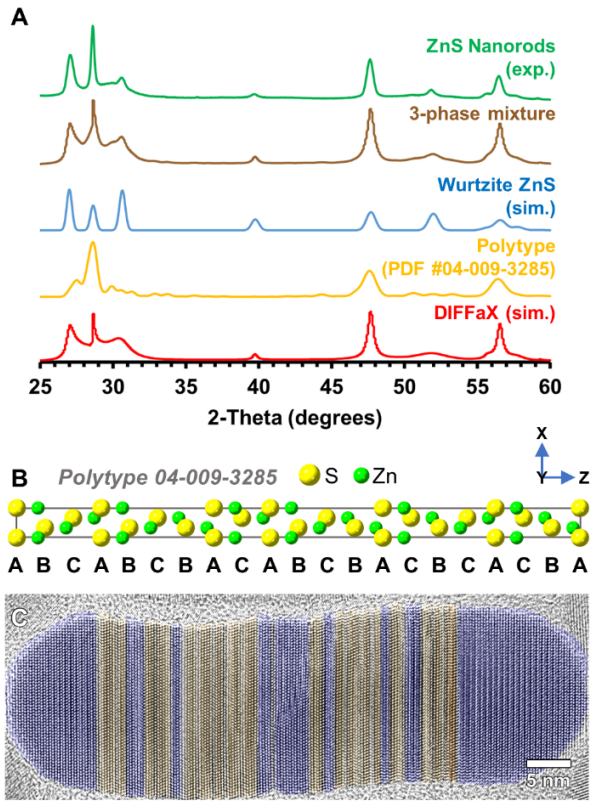

Figure 3. (A) Experimental XRD pattern of ZnS nanorods (reproduced from Figure 1) compared with the simulated pattern for the three-phase mixture. Patterns corresponding to the individual components of the three-phase mixture (wurtzite, polytype PDF 04-009-3285, and DIFFAX model) are also shown. (B) Unit cell of polytype PDF 04-009-3285 indicating stacking sequence. (C) False-colored HRTEM image of a ZnS nanorod highlighting wurtzite (blue) and zincblende (orange) regions.

The three-phase model accounts for all observed features in the experimental XRD pattern. It supports the presence of stacking faults in the bulk of the sample and the formation of a complex ZnS polytype, which has not been observed previously during nanoparticle cation exchange reactions. To help rationalize how a high density of stacking faults emerges, we consider unique aspects of the roxbyite crystal structure that likely contribute. Roxbyite contains a distorted hcp anion sublattice,[33] while wurtzite has an hcp sublattice without distortion (Figure S6). To transform from distorted to regular hcp during cation exchange, many of the anions have to shift positions slightly, concomitantly with the migration and replacement of cations in the structure. The most likely diffusion channels where Zn^{2+} would enter the $Cu_{1.8}S$ nanorods are along the sides of the nanorods, as these are where the cation vacancies are located.[4,34] Rapid diffusion and cation exchange will result in anions shifting positions, transforming from distorted hcp to regular hcp. We postulate that during this transformation, the planes can slip slightly to form stacking faults. Residual Cu^{+} is near background levels and not concentrated at stacking faults (Figure S3), suggesting that it does not contribute significantly to stacking fault formation.

The formation of stacking faults by cation exchange is inherently interesting, but it is also important for future efforts to control properties, as stacking faults can cause red shifting of cathodoluminescence emission[23,35] lead to shifting of photoluminescence emission peaks.[22] We therefore sought to synthetically tune the density of stacking faults so that they could be minimized. Building off of our proposed pathway for how stacking faults emerge, we focused on slowing the rate of cation exchange by decreasing the rate at which $ZnCl_2$ was added and decreasing the temperature. These modifications would also decrease the ability of the close-packed planes to slip, as the disruption to the structure through cation migration and thermal motion would be decreased.

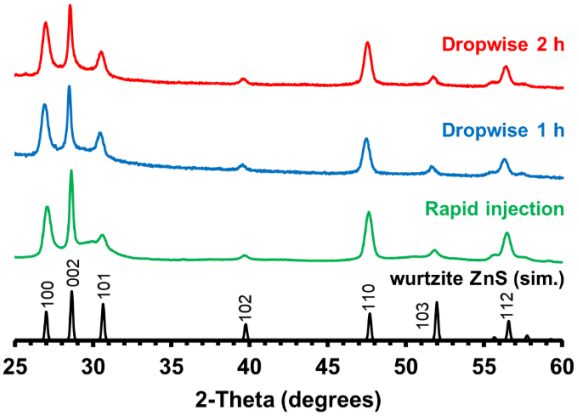

Figure 4. XRD patterns of ZnS nanorods formed from rapid $ZnCl_2$ injection (reproduced from Figure 1) compared to dropwise over 1 h and 2 h. A simulated pattern for wurtzite ZnS with 30% preferred orientation along [001] is shown for comparison.[36]

Keeping the temperature and overall amount of $ZnCl_2$ constant, we slowly injected the $ZnCl_2$ exchange solution using a syringe pump, rather than rapid injection as was used previously (Figure 4). Adding the $ZnCl_2$ dropwise over 1 h decreased the intensity of the peak at 29 º2θ, which is characteristic of the ZnS polytype. Adding the $ZnCl_2$ even slower – dropwise over 2 h – further decreased the intensity of the polytype peak. However, the relative ratios of the wurtzite 100 and 101 peaks remain unchanged and the <101> peaks remain suppressed. Decreasing the rate of exchange through reagent injection prevents the stacking faults from ordering, and therefore the polytype from forming, but it does not significantly decrease the overall density of stacking faults based on TEM (Figure S7) and XRD data, as features related to the presence of stacking faults still remain. However, by keeping the rapid injection but decreasing the temperature from 120 ºC to 80 ºC, the stacking fault density did appear to decrease significantly, based on the XRD pattern in Figure 5. The peak at 29 º2θ that is characteristic of the ordered polytype is no longer observed and the intensities of the peaks shared by both wurtzite and zincblende decrease in intensity, becoming more in line with that expected for wurtzite. The accompanying HRTEM images in Figures 5 and S8 microscopically validate the bulk XRD data. The higher-temperature sample has a higher stacking fault density and evidence of ordered polytype formation, while the lower-temperature sample has a much lower stacking fault density and no evidence of an ordered polytype. Zn^{2+} exchange at temperatures higher than 120 °C showed no notable changes (Figure S9). Interestingly, annealing the ZnS nanorods having a high stacking fault density in an evacuated, sealed ampoule for 5 h at 750 ºC does not appear to modify them. The stacking faults persist, based on TEM and XRD data (Figure S10), and therefore are locked in place once formed.

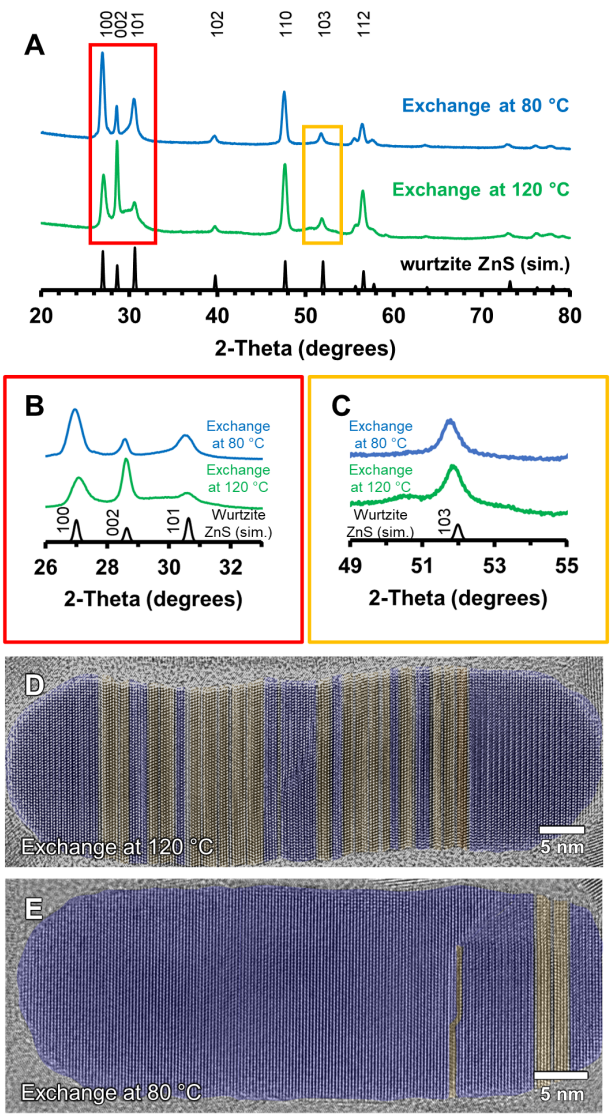

Figure 5. (A) XRD patterns of ZnS nanorods synthesized by cation exchange at 120 ºC (reproduced from Figure 1) and 80 ºC. A simulated pattern for wurtzite ZnS is shown for comparison. Expanded regions (B, C) highlight key differences between samples. False-colored HRTEM images showing wurtzite (blue) and zincblende (orange) regions are shown for the exchanges at (D) 120 °C (reproduced from Figure 3C for comparison) and (E) 80 °C.

The observation that a high density of stacking faults forms during cation exchange, a common post-synthetic modification pathway for nanoparticles, is an important addition to our knowledge of how these reactions occur. Such behavior suggests that the anion sublattice is more dynamic than previously recognized, and most significantly, that the close-packed planes are capable of slipping locally, including in ways that result in the formation of complex ordered polytypes. As demonstrated here, the ability to synthetically tune stacking fault density is also important. Their presence can impact properties – sometimes detrimentally, as in photoluminescence,[22] and sometimes advantageously, as in catalysis[37] – and modifying them once they form by cation exchange has not been successful.

ASSOCIATED CONTENT

Supporting Information

The Supporting Information is available free of charge on the ACS Publications website.

Complete experimental details and additional electron microscopy and X-ray diffraction data (PDF)

AUTHOR INFORMATION

Corresponding Author

* res20@psu.edu

Notes

The authors declare no competing financial interests.

ACKNOWLEDGMENT

This work was supported by the U.S. National Science Foundation under grant DMR-1904122. TEM/STEM imaging, EDS mapping, and X-ray diffraction were at the Materials Characterization Lab of the Penn State Materials Research Institute.

REFERENCES

(1) Robinson, R. D.; Sadtler, B.; Demchenko, D. O.; Erdonmez, C. K.; Wang, L.-W.; Alivisatos, A. P., Spontaneous Superlattice Formation in Nanorods Through Partial Cation Exchange. *Science* **2007**, *317*, 355-358.

(2) De Trizio, L.; Manna, L., Forging Colloidal Nanostructures via Cation Exchange Reactions. *Chem. Rev.* **2016**, *116*, 10852-10887.

(3) Fenton, J. L.; Steimle, B. C.; Schaak, R. E., Tunable intraparticle frameworks for creating complex heterostructured nanoparticle libraries. *Science* **2018**, *360*, 513-517.

(4) Steimle, B. C.; Fenton, J. L.; Schaak, R. E., Rational construction of a scalable heterostructured nanorod megalibrary. *Science* **2020**, *367*, 418-424.

(5) Butterfield, A. G.; Steimle, B. C.; Schaak, R. E., Retrosynthetic Design of Morphologically Complex Metal Sulfide Nanoparticles Using Sequential Partial Cation Exchange and Chemical Etching. *ACS Materials Lett.* **2020**, *2*, 1106-1114.

(6) Beberwyck, B. J.; Surendranath, Y.; Alivisatos, A. P., Cation Exchange: A Versatile Tool for Nanomaterials Synthesis. *J. Phys. Chem. C* **2013**, *117*, 19759-19770.

(7) Fenton, J. L.; Steimle, B. C.; Schaak, R. E., Structure-Selective Synthesis of Wurtzite and Zincblende ZnS, CdS, and $CuInS_2$ Using Nanoparticle Cation Exchange Reactions. *Inorg. Chem.* **2019**, *58*, 672-678.

(8) Hernández-Pagán, E. A.; O'Hara, A.; Arrowood, S. L.; McBride, J. R.; Rhodes, J. M.; Pantelides, S. T.; Macdonald, J. E., Transformation of the Anion Sublattice in the Cation-Exchange Synthesis of Au_2S from $Cu_{2-x}S$ Nanocrystals. *Chem. Mater.* **2018**, *30*, 8843-8851.

(9) Ha, D.-H.; Caldwell, A. H.; Ward, M. J.; Honrao, S.; Mathew, K.; Hovden, R.; Koker, M. K. A.; Muller, D. A.; Hennig, R. G.; Robinson, R. D., Solid–Solid Phase Transformations Induced through Cation Exchange and Strain in 2D Heterostructured Copper Sulfide Nanocrystals. *Nano Lett.* **2014**, *14*, 7090-7099.

(10) Son, D. H.; Hughes, S. M.; Yin, Y.; Paul Alivisatos, A., Cation Exchange Reactions in Ionic Nanocrystals. *Science* **2004**, *306*, 1009-1012.

(11) Li, H.; Brescia, R.; Povia, M.; Prato, M.; Bertoni, G.; Manna, L.; Moreels, I., Synthesis of Uniform Disk-Shaped Copper

Telluride Nanocrystals and Cation Exchange to Cadmium Telluride Quantum Disks with Stable Red Emission. *J. Am. Chem. Soc.* **2013**, *135*, 12270-12278.

(12) Ramirez, O.; Ramasamy, P.; Chan Choi, Y.; Lee, J.-S., Morphology Transformation of Chalcogenide Nanoparticles Triggered by Cation Exchange Reactions. *Chem. Mater.* **2019**, *31*, 268-276.

(13) Le, H. K. D.; Xiong, H.; Page, B. A.; Garcia-Herrera, L. F.; McAllister, H. P.; Li, B. C.; Wang, H.; Plass, K. E., Effects of I_2 on $Cu_{2-x}S$ Nanoparticles: Enabling Cation Exchange but Complicating Plasmonics. *ACS Materials Lett.* **2020**, *2*, 140-146.

(14) Steimle, B. C.; Lord, R. W.; Schaak, R. E., Phosphine-Induced Phase Transition in Copper Sulfide Nanoparticles Prior to Initiation of a Cation Exchange Reaction. *J. Am. Chem. Soc.* **2020**, *142*, 13345-13349.

(15) Huang, F.; Banfield, J. F., Size-Dependent Phase Transformation Kinetics in Nanocrystalline ZnS. *J. Am. Chem. Soc.* **2005**, *127*, 4523-4529.

(16) Wang, Z.; Daemen, L. L.; Zhao, Y.; Zha, C. S.; Downs, R. T.; Wang, X.; Wang, Z. L.; Hemley, R. J., Morphology-tuned wurtzite-type ZnS nanobelts. *Nat. Mater.* **2005**, *4*, 922-927.

(17) Pan, Z. W.; Dai, Z. R.; Wang, Z. L., Nanobelts of Semiconducting Oxides. *Science* **2001**, *291*, 1947-1949.

(18) Joyce, H. J.; Wong-Leung, J.; Gao, Q.; Tan, H. H.; Jagadish, C., Phase Perfection in Zinc Blende and Wurtzite III–V Nanowires Using Basic Growth Parameters. *Nano Lett.* **2010**, *10*, 908-915.

(19) Biswas, S.; Kar, S., Fabrication of ZnS nanoparticles and nanorods with cubic and hexagonal crystal structures: a simple solvothermal approach. *Nanotechnology* **2008**, *19*, 045710.

(20) Zhang, Q.; Yin, K.; Dong, H.; Zhou, Y.; Tan, X.; Yu, K.; Hu, X.; Xu, T.; Zhu, C.; Xia, W.; Xu, F.; Zheng, H.; Sun, L., Electrically driven cation exchange for in situ fabrication of individual nanostructures. *Nat. Commun.* **2017**, *8*, 14889.

(21) Denzler, D.; Olschewski, M.; Sattler, K., Luminescence studies of localized gap states in colloidal ZnS nanocrystals. *J. Appl. Phys.* **1998**, *84*, 2841-2845.

(22) Spirkoska, D.; Arbiol, J.; Gustafsson, A.; Conesa-Boj, S.; Glas, F.; Zardo, I.; Heigoldt, M.; Gass, M. H.; Bleloch, A. L.; Estrade, S.; Kaniber, M.; Rossler, J.; Peiro, F.; Morante, J. R.; Abstreiter, G.; Samuelson, L.; Fontcuberta i Morral, A., Structural and optical properties of high quality zinc-blende/wurtzite GaAs nanowire heterostructures. *Phys. Rev. B* **2009**, *80*, 245325.

(23) Liu, B. D.; Yang, B.; Dierre, B.; Sekiguchi, T.; Jiang, X., Local defect-induced red-shift of cathodoluminescence in individual ZnS nanobelts. *Nanoscale* **2014**, *6*, 12414-12420.

(24) Hughes, S. M.; Alivisatos, A. P., Anisotropic Formation and Distribution of Stacking Faults in II–VI Semiconductor Nanorods. *Nano Lett.* **2013**, *13*, 106-110.

(25) Steimle, B. C.; Fagan, A. M.; Butterfield, A. G.; Lord, R. W.; McCormick, C. R.; Di Domizio, G. A.; Schaak, R. E., Experimental Insights into Partial Cation Exchange Reactions for Synthesizing Heterostructured Metal Sulfide Nanocrystals. *Chem. Mater.* **2020**, *32*, 5461-5482

(26) Ding, Y.; Wang, Z. L., Structure Analysis of Nanowires and Nanobelts by Transmission Electron Microscopy. *J. Phys. Chem. B* **2004**, *108*, 12280-12291.

(27) Moore, D.; Wang, Z. L., Growth of anisotropic one-dimensional ZnS nanostructures. *J. Mater. Chem.* **2006**, *16*, 3898-3905.

(28) Treacy, M. M. J.; Newsam, J. M.; Deem, M. W., A general recursion method for calculating diffracted intensities from crystals containing planar faults. *Proc. R. Soc. Lond. A* **1991**, *433*, 499-520.

(29) Mardix, S., Polytypism: A controlled thermodynamic phenomenon. *Phys. Rev. B* **1986**, *33*, 8677-8684.

(30) Boutaiba, F.; Belabbes, A.; Ferhat, M.; Bechstedt, F., Polytypism in ZnS, ZnSe, and ZnTe: First-principles study. *Phys. Rev. B* **2014**, *89*, 245308.

(31) Mardix, S.; Alexander, E.; Brafman, O.; Steinberger, I. T., Polytype families in zinc sulphide crystals. *Acta Cryst.* **1967**, *22*, 808-812.

(32) Tiwary, C. S.; Srivastava, C.; Kumbhakar, P., Onset of sphalerite to wurtzite transformation in ZnS nanoparticles. *J. Appl. Phys.* **2011**, *110*, 034908.

(33) Xia, Y.; Gilroy, K. D.; Peng, H.-C.; Xia, X., Seed-Mediated Growth of Colloidal Metal Nanocrystals. *Angew. Chem., Int. Ed.* **2017**, *56*, 60-95.

(34) Lesnyak, V.; Brescia, R.; Messina, G. C.; Manna, L., Cu Vacancies Boost Cation Exchange Reactions in Copper Selenide Nanocrystals. *J. Am. Chem. Soc.* **2015**, *137*, 9315-9323.

(35) Liu, R.; Bell, A.; Ponce, F. A.; Chen, C. Q.; Yang, J. W.; Khan, M. A., Luminescence from stacking faults in gallium nitride. *Appl. Phys. Lett.* **2005**, *86*, 021908.

(36) Holder, C. F.; Schaak, R. E., Tutorial on Powder X-ray Diffraction for Characterizing Nanoscale Materials. *ACS Nano* **2019**, *13*, 7359-7365.

(37) Bornovski, R.; Huang, L.-F.; Komarala, E. P.; Rondinelli, J. M.; Rosen, B. A., Catalytic Enhancement of CO Oxidation on LaFeO_3 Regulated by Ruddlesden–Popper Stacking Faults. *ACS Appl. Mater. Interfaces* **2019**, *11*, 33850-33858.

Insert Table of Contents artwork here